Overt and hidden polymorphism in the binary system involving the Z- and E- isomers of broparestrol

Siro Toscani, Hassan Allouchi, René Ceolin, Laia Villalobos, Maria Barrio, Josep-Lluis Tamarit, Ivo Rietveld

International Journal of Pharmaceutics 669 (2025) 125060

Contents lists available at ScienceDirect

International Journal of Pharmaceutics

journal homepage: www.elsevier.com/locate/ijpharm

Overt and hidden polymorphism in the binary system involving the *Z*- and *E*- isomers of broparestrol

Siro Toscani [a], Hassan Allouchi [b], René Ceolin [c], Laia Villalobos [c], Maria Barrio [c], Josep-Lluis Tamarit [c], Ivo B. Rietveld [d,*]

[a] *Institut des Sciences Chimiques de Rennes – UMR 6226, Faculté des Sciences, Université de Rennes 1, Bâtiment 10B. 263, Avenue du Général Leclerc 35042, Rennes, France*
[b] *EA 7502 SIMBA, Laboratoire de Chimie Physique, Faculté de Pharmacie, Université de Tours 31, Avenue Monge 37200, Tours, France*
[c] *Grup de Caracterització de Materials, Departament de Física and Barcelona Research Center in Multiscale Science and Engineering, Universitat Politècnica de Catalunya, EEBE, Campus Diagonal-Besòs, Av. Eduard Maristany 10-14 08019, Barcelona, Catalunya, Spain*
[d] *Laboratoire SMS, UR 3233, Université de Rouen Normandie, Normandie Université, F76000, Rouen, France*

A R T I C L E I N F O

Keywords:
Broparestrol
Polymorphism
Stereoisomers
Phase behaviour
Binary mixtures
Thermodynamics
Crystal structure

A B S T R A C T

Broparestrol has been used as a drug to treat acne in the form of a mixture of its two stereoisomers. Although it has been withdrawn from the market, the binary system is rich in polymorphism and understanding the phase behaviour of the binary system involving the *E*- and *Z*-isomers is challenging. Physical mixtures do not immediately give rise to equilibrium phase behaviour, whereas recrystallization often leads to metastable phases and the appearance of stable phases can take years. A new polymorph of *E*-broparestrol has been found crystallizing in a monoclinic unit cell, space group $P2_1/c$, with lattice parameters $a = 5.6079(4)$ Å, $b = 16.1206(10)$ Å, $c = 20.250\ (1)$ Å, $\beta = 100.569(4)^\circ$, $V_{cell} = 1799.6(2)$ Å^3, and $Z = 4$. This polymorph, I_E, is stable at high temperatures, whereas the published form, II_E, is stable at room temperature. In the case of *Z*-broparestrol polymorphism has been observed too; however, it has so far only occurred within the binary phase diagram, and it has not been possible to isolate the new polymorph of *Z*-broparestrol, II_Z. Through the phase behaviour in the binary system, it could be determined that the new *Z* polymorph, II_Z, behaves monotropically in relation to the known triclinic polymorph of the *Z*-isomer, I_Z. Nothing is known about its structure, and it is therefore not clear yet whether II_Z may possess a stable domain under pressure. A stable temperature-composition phase diagram of the binary system containing *E*- and *Z*-broparestrol is proposed.

1. Introduction

To control the physical–chemical properties and the pharmaceutical activity of active pharmaceutical ingredients (APIs), binary or even highter multicomponent systems are important. Such systems facilitate increasing the solubility and bioavailability of the APIs in the system through cocrystals (Bolla and Nangia, 2016; Qiao et al., 2011) or glass-forming mixtures, (Kawakami et al., 2014; Kissi et al., 2019; Valenti et al., 2023; Jain et al., 2015; Nyamba et al., 2021) for example. On the other hand, in the case of enantiomers, binary systems may need to be separated into single pure antipodes because of a difference in pharmaceutical activity or undesirable side effects. (Johnston et al., 2023; Mutiti et al., 2021) In such cases, the relative stability of the equimolar composition as racemate or conglomerate is relevant, as only conglomerates can be easily separated. (Jacques et al., 1994; Coquerel, 2006; Rietveld et al., 2012) From a more fundamental point of view, the study of multicomponent systems can reveal the existence of metastable polymorphs that do not crystallize easily or not at all in unary systems. (Haget et al., 1999; Brandel et al., 2013) In such cases, through extrapolation of two-phase equilibria in a multicomponent system, thermodynamic properties that otherwise cannot be obtained can be inferred. (Barrio et al., 2002; Pardo et al., 2001; Pardo et al., 2005).

The synthesis of broparestrol, 1-(2-bromo-1,2-diphenylethenyl)-4-ethylbenzene ($C_{22}H_{19}Br$, $M = 363.29$ g·mol^{-1}, chemical formulas in Fig. 1) was first reported by Buu Hoï in 1946 and later by Al-Hassan in 1987. (Buu Hoï, 1946; Al-Hassan, 1987; Al-Hassan, 1987) Broparestrol possesses two isomers *E* and *Z* as indicated in Fig. 1. The $Z/E \approx 40/60$ mixture has been used in dermatology as the active component of

* Corresponding author.
E-mail address: ivo.rietveld@univ-rouen.fr (I.B. Rietveld).

https://doi.org/10.1016/j.ijpharm.2024.125060
Received 24 October 2024; Received in revised form 5 December 2024; Accepted 6 December 2024
Available online 13 December 2024

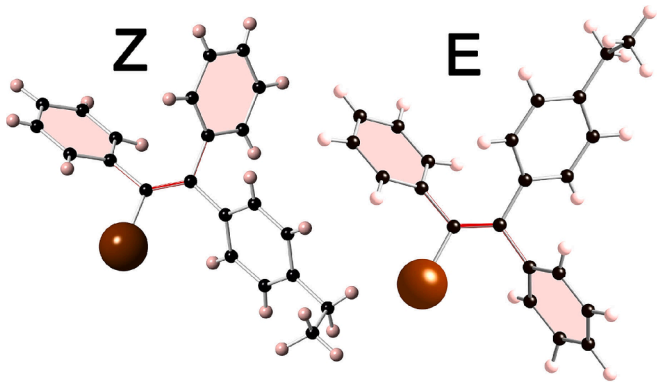

Fig. 1. Molecular structures of the *Z*-(cis) and *E*-(trans) isomers of broparestrol ($C_{22}H_{19}Br$, M = 363.31 g/mol). The unsubstituted phenyl rings (pink surfaces) are located on the same side of the (red) C = C double bond in the *Z*-isomer and on the opposite side of the C = C bond in the *E*-isomer. The *Z*- and *E*-isomers have been drawn using the SAXGED and BEPPET files of the Cambridge Structural Database, respectively.

ointments and solutions against acne. The isomers were isolated by fractional crystallization (Laroche, 1978) but never marketed, although the *E*-isomer was shown to inhibit prolactin-induced mammary cancer. (Laroche, 1978; Drosdowsky et al., 1980) Broparestrol has eventually been withdrawn from the European market.

The binary system formed by *E*- and *Z*-broparestrol mixtures is investigated in the current paper for two reasons. First, it is an interesting example to demonstrate the influence of metastable polymorphs on binary phase equilibria. Secondly, it appears that the isomer mixtures facilitate the appearance and possible stabilization of metastable polymorphs.

This paper contains two parts. The first part demonstrates and characterizes the dimorphism of the *E*-isomer of broparestrol, and the second part is devoted to the phase equilibria in the binary *T-x* phase diagram involving the two isomers. Three partially metastable phase diagrams are found with which a stable phase diagram is constructed. Moreover, the existence of a metastable polymorph of the *Z*-isomer is demonstrated.

Two crystal structures of broparestrol have been previously determined: *E*- and *Z*-broparestrol have been found to crystallize in the monoclinic system, space group $P2_1/c$, (Fornies-Marquina et al., 1972) and the triclinic system, space group *P*-1, (Rodier et al., 1989) for form II_E and form I_Z, respectively. In both structures, molecules are held together by van der Waals interactions and, at room temperature, their specific volumes are virtually the same: 441.1 Å^3 and 441.6 Å^3 per molecule for the *E*- and *Z*-isomers, respectively.

2. Materials and methods

2.1. Broparestrol

Pure form II_E and form I_Z of broparestrol isomers (purities > 99 %) were supplied by Devimy Laboratory (France) and used as such after X-ray diffraction showed experimental patterns in fair agreement with the ones calculated from the crystal structures present in the Cambridge Crystallographic Database (CSD): BEPPET (*E*-isomer) and SAXGET (*Z*-isomer) (**Figure S1** in the **Supplementary Materials**).

2.2. High-resolution powder X-ray diffraction

Powder X-ray diffraction (PXRD) patterns have been obtained in transmission mode with two high-resolution diffractometers from INEL (France) equipped with position sensitive detectors CPS120 in the Debye-Scherrer geometry. Monochromatic Cu-Kα_1 (λ = 1.54056 Å) radiation was selected by means of a focusing incident-beam germanium monochromator. Samples were introduced in 0.5 mm-diameter Lindemann capillaries, which were rotated perpendicularly to the X-ray beam during the data acquisition to improve the averaging over the crystallite orientations. Cubic $Na_2Ca_3Al_2F_4$ was used for external calibration.

Long acquisitions were carried out at 293 K, while measurements as a function of temperature were carried out using a liquid nitrogen 700 series Cryostream Cooler from Oxford Cryosystems. Before each isothermal data acquisition, the specimen was allowed to equilibrate for about 10 min, and each acquisition time was no less than 1 h. The heating rate in-between data collection was 1.33 K min^{-1}. Patterns were recorded on heating in the temperature range from 130 K up to the melting points. The PEAKOC application from the DIFFRACTINEL software was used for the calibration as well as for the peak position determinations after pseudo-Voigt fittings. Lattice parameters were refined using TOPAS-Academic. (Coelho, 2007; Coelho, 2018).

2.3. Structure solution from powder diffraction

For structure solution of a new *E*-broparestrol polymorph, form I_E, with a pattern obtained at 293 K, the programs *DASH* (David et al., 2006) and *TOPAS-Academic* (Coelho, 2007; Coelho, 2018) were employed, and the powder pattern was truncated to 29.6° in 2θ (Cu Kα_1), corresponding to a real-space resolution of 3.01 Å. The background was subtracted with a Bayesian high-pass filter. (David and Sivia, 2001) Peak positions for indexing were obtained by fitting with an asymmetry-corrected pseudo-Voigt function. (Finger et al., 1994; Thompson et al., 1987) 21 peaks were indexed with the program *DICVOL*91. (Boultif and Louër, 1991) This did not lead to any promising unit cell. With TOPAS, (Coelho, 2003) several different settings of a monoclinic unit cell ($P2_1$) with a volume of 1802 Å^3 were obtained with the highest probability, similar to the volume of the known structure (BEPPET). Pawley refinement was carried out with DASH to extract integrated intensities and their correlations, from which the space group was determined using Bayesian statistical analysis. (Markvardsen et al., 2001) $P2_1/c$ was returned as the most probable space group. It was the space group with the highest symmetry and the other known structure of *E*-broparestrol (BEPPET) has this space group too. (Fornies-Marquina et al., 1972) It resulted in a Pawley χ^2 of 17.88. The high value for the Pawley χ^2 may be due to phase impurity. Simulated annealing was used to solve the crystal structure from the powder pattern in direct space. The starting molecular geometry was taken from the published polymorph from the CSD (reference code BEPPET). (Fornies-Marquina et al., 1972) This geometry was then optimized using the COMPASS forcefield (v2.8) in the Materials Studio Forcite Geometry Optimization module with the extrafine setting and Ewald summation. In 30 simulated annealing runs, the same crystal structure was found 30 times. The profile χ^2 of the best solution was 67.66, which is less than four times the Pawley χ^2; this is a good indication that the correct solution has been found.

For the Rietveld refinement, data out to 75 °2θ were used, which corresponds to 1.27 Å real-space resolution. The Rietveld refinement was carried out with *TOPAS-Academic*. (Coelho, 2007; Coelho, 2018) Bond lengths, bond angles and planar groups were subjected to suitable restraints, including bonds to H atoms. A global B_{iso} was refined for all non-hydrogen atoms, with the B_{iso} of the hydrogen atoms constrained at 1.2 times the value of the global B_{iso}. The molecular geometry was checked with *Mogul*, (Bruno et al., 2004) which compares each bond length and bond angle to corresponding distributions from single-crystal data. A final optimization of the molecule was carried out with the COMPASS (v2.8) force field. A fit of the powder data is provided in **Figure S2** in the **Supplementary Materials**.

Supplementary crystallographic data can be found in the CCDC, deposition number 2393322, and obtained free of charge from the Cambridge Crystallographic Data Centre via https://www.ccdc.cam.ac.uk/structures/.

2.4. Differential scanning calorimetry

2.4.1. Equipment

Differential scanning calorimetry (DSC) experiments have been performed with the DSC-cell of a TA2000 thermal analyzer from TA-Instruments (USA), calibrated using the temperature and heat of fusion of indium.

2.4.2. Study of the binary system involving the Z- and E-isomers of broparestrol

To explore the binary system involving the two isomers, physical mixtures in different ratios, weighed using a balance sensitive to 0.01 mg, were introduced in aluminum pans with which three series of DSC experiments were performed:

(1) First, after a one-week annealing at 323 K, the samples, II_E and I_Z, were heated at a rate of 5 K min^{-1} under a nitrogen flux from room temperature up to complete melting, leading to a first temperature-composition (*T-x*) phase diagram exhibiting a eutectic equilibrium ε_1 with an onset temperature at 363 K.

(2) Second, after cooling to 298 K and storing the samples for three years at room temperature, they were reheated at the same rate, leading to a second *T-x* phase diagram exhibiting the eutectic equilibrium ε_2 with an onset temperature at 358 K.

(3) A third series of experiments was carried out with mixtures of forms II_E and I_Z that were first molten and subsequently cooled to room temperature. Soon after recrystallization had taken place, they were reheated, leading to a third *T-x* phase diagram exhibiting the eutectic equilibrium ε_3 with an onset at 340 K. Moreover, some specimens stored for three years at room temperature (series 2) also exhibited the same eutectic equilibrium ε_3.

The temperatures of the invariant (eutexy) and monovariant (liquidus) equilibria were taken at the onset and the maximum of the related DSC peaks, respectively.

3. Results and discussion

3.1. Dimorphism of E-broparestrol

3.1.1. Calorimetric studies of E-broparestrol

DSC experiments were performed using the as-received form II_E, which was found to melt at $T_{fus,\ II\text{-}E} = 385.4(1.0)$ K (onset) with a melting enthalpy of $\Delta_{fus}H_{II\text{-}E} = +\ 90.8(1.8)$ J/g. By slowly cooling the melt, recrystallization was found to occur at $T_{cryst} = 360.3$ K (onset) with a crystallization enthalpy of $\Delta_{cryst}H = -66.6$ J/g. Heating again, the melting temperature was found to be 386.7(1.0) K, which is close to the value obtained previously; however, the value of the melting enthalpy was + 79.4(1.6) J/g, i. e. smaller than the initial melting enthalpy by 11.4 J/g (see Fig. 2**A**).

Because these results could be related to dimorphism, a powder of form II_E was introduced in a Lindemann capillary for an examination by powder X-ray diffraction. After heating the sample up to fusion and slow cooling to room temperature, recrystallization occurred within a few minutes. The X-ray pattern, obtained after about 1 h of data collection, was different from that of the as-received form II_E, thus structurally corroborating the existence of dimorphism for *E*-broparestrol (Fig. 2**B**). However, further X-ray diffraction experiments performed 24 h later showed that the new phase slowly reverted to the known phase II_E upon standing at room temperature.

In a different experiment, the melt is reheated from the glassy state after quenching it at 213 K, which results in the DSC curve presented in Fig. 3. In the resulting DSC curve, first, a glass transition at $T_g = 264$ K (midpoint) can be observed. It is followed by an exothermic effect 'a' with an onset at 300.5 K indicating a recrystallization process and subsequently by a broad endothermic peak 'b' starting at about 310 K ($\Delta_{a+b}H = 12.8$ J/g). Finally, a double melting peak 'c1 + c2′ is observed with onsets at 384.4 K and 386 K, respectively, corresponding to a heat of fusion of $\Delta_{c1+c2}H = 84.5$ J/g, i.e. a value ranging between those of the known II_E form and the new I_E. Moreover, the glass transition temperature obeys the empirical Tammann rule according to which the ratio

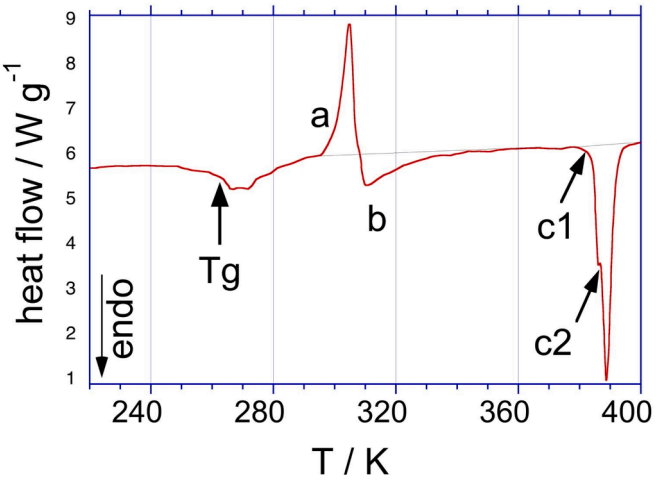

Fig. 3. DSC curve recorded on reheating from the glass phase obtained after quenching a molten sample of *E*-broparestrol at 213 K at a heating rate of 5 K min^{-1} (T_g = glass transition).

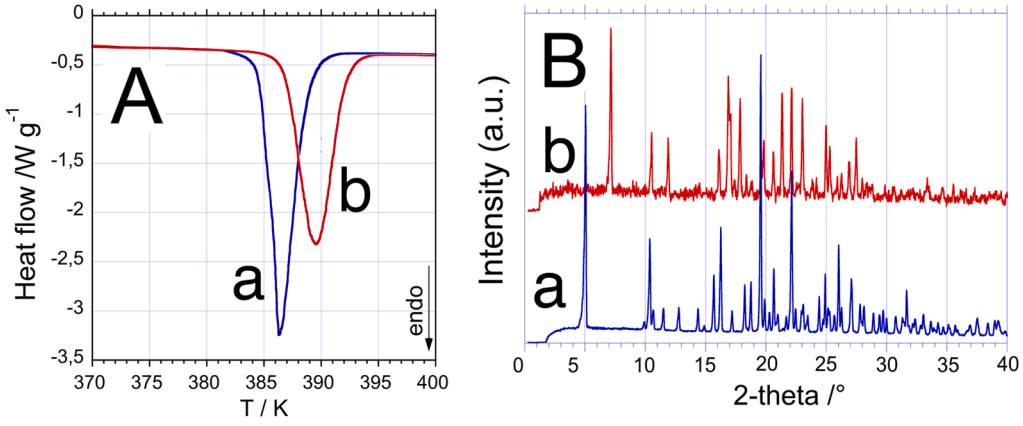

Fig. 2. Confirmation of the dimorphism of *E*-broparestrol. **(A)** DSC curves (a) obtained on heating an as-received monoclinic II_E form (4.71 mg) of *E*-broparestrol at 5 K min^{-1} and (b) obtained on reheating the same sample at the same rate after recrystallisation on slow cooling. **(B)** Room temperature X-ray diffraction patterns for (a) the as-received form II_E (BEPPET), and (b) the new phase, form I_E, recrystallized while slowly cooling the melt to room temperature.

T_g/T_{fus} is in the order of 2/3. In the present case, the ratio equals 0.683.

To verify the hypothesis of a possible recrystallization of a mixture of phases that could explain the double melting peak in Fig. 3, the following X-ray diffraction experiment was performed several times: form II_E in a capillary was molten *in situ* then quickly cooled to room temperature and, when recrystallization started, the recorded X-ray patterns demonstrated the existence of a mixture of two phases, the known form II_E and the new form I_E in various ratios (**Figure S3** in the **Supplementary Materials**). Because the melting temperature of the new phase was found to be higher, this phase was labelled 'form I_E' and the known monoclinic phase 'form II_E'. From these experiments, it was also concluded that on slow cooling the melt crystallizes into form I_E, while on quenching and reheating the glass phase, mixtures of the two forms in various ratios are obtained.

To investigate whether these polymorphs are enantiotropically or monotropically related, the temperature of transition from form II_E to form I_E was calculated with the formula proposed by Yu, (Yu, 1995) neglecting the contribution of the specific heats:

$$T_{II\rightarrow I} = \frac{\Delta_{fus}H_I - \Delta_{fus}H_{II}}{\frac{\Delta_{fus}H_I}{T_{fus,I}} - \frac{\Delta_{fus}H_{II}}{T_{fus,II}}} \quad (1)$$

With $\Delta_{fus}H_{I\text{-}E} = 79.4$ J/g, $\Delta_{fus}H_{II\text{-}E} = 90.8$ J/g, $T_{fus,I\text{-}E} = 386.7$ K and $T_{fus,II\text{-}E} = 385.4$ K, one obtains $T_{II\text{-}E\rightarrow I\text{-}E} = 376.6$ K with $\Delta_{II\text{-}E\rightarrow I\text{-}E}H = +11.4$ J/g deduced from Hess' law. Using the Clausius-Clapeyron equation, the same result of 376.6 K is found for the temperature of the I_E-II_E-vapour triple point (**Table S1** in the **Supplementary Materials**) together with an estimate of the vapour pressure.

It can therefore be concluded that the $II_E \rightarrow I_E$ transition occurs endothermically on heating below the melting temperature, thus indicating that the two forms are enantiotropically related: form I_E being more stable at high temperature and form II_E being more stable at low temperature.

3.1.2. *Crystal structure of the E-broparestrol high-temperature form I_E*

The Rietveld refinement of the high-resolution powder X-ray diffraction pattern obtained at 293 K progressed smoothly and produced a good fit with $\chi^2 = 4.322$, $R'_p = 20.413$, $R'_{wp} = 22.321$ (values after background correction), $R_p = 6.300$ and $R_{wp} = 8.786$ (values before background subtraction). B_{iso} refined to 11.3(3) Å^2. Additional refinement information can be found in **Table S2** in the **Supplementary Materials**.

The crystal structure of form I_E was found to be monoclinic, space group $P2_1/c$, with lattice parameters $a = 5.6079(4)$ Å, $b = 16.1206(10)$ Å, $c = 20.250$ (1) Å, $\beta = 100.569(4)°$, $V_{cell} = 1799.6(2)$ Å^3, and $Z = 4$. A projection of the unit-cell on the **bc** plane is shown in **Figure S4a** and the atom numbering in **Figure S4b**. Atom coordinates and atomic displacement parameters have been compiled in **Table S3** in the **Supplementary Materials**. Bond lengths, bond angles, and torsion angles can be found in **Tables S4, S5 and S6**, respectively.

The lattice parameters of the low-temperature form II_E were determined by Rietveld refinement using a PXRD pattern recorded at the same temperature of 293 K with the same diffractometer as used for form I_E. Starting from the previously reported structure, (Fornies-Marquina et al., 1972) results were as follows: $a = 8.5774(6)$ Å, $b = 35.819(3)$ Å, $c = 5.7545(4)$ Å, $\beta = 86.151(6)°$, $V_{cell} = 1764.0(2)$ Å^3, and $Z = 4$. Comparing the cell volumes of forms I_E and II_E demonstrates that the low-temperature form II_E has a higher density than form I_E. In both cases, intermolecular interactions consist mainly of van der Waals interactions, while the polymorphism is the result of conformational changes, as shown in Fig. 4, in which the substituted phenyl-rings of the two forms are superimposed.

3.1.3. *Thermal expansion of the E-broparestrol polymorphs and of the triclinic Z-broparestrol isomer*

Lattice parameters, volumes of the asymmetric unit, and specific volumes of *E*-broparestrol forms I and II, together with those of the triclinic *Z*-broparestrol as a function of temperature have been compiled in **Tables S7, S8 and S9** in the **Supplementary Materials**, respectively.

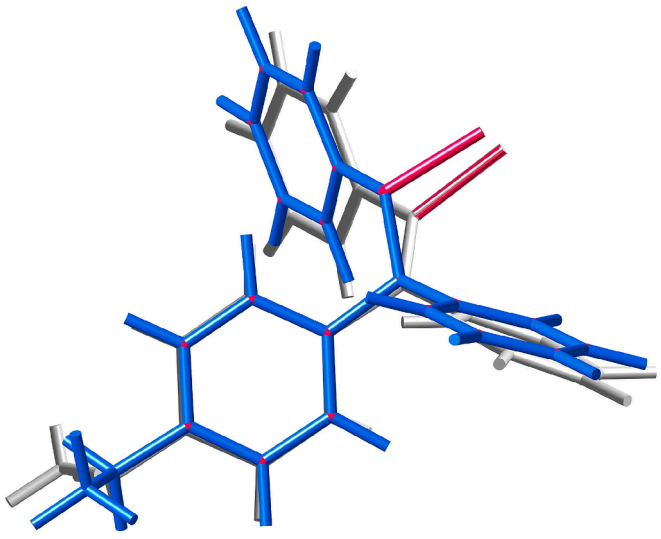

Fig. 4. Overlay of the *E*-broparestrol molecules of form I_E (blue) and form II_E (grey) with C-Br bonds in pink. The substituted central phenyl rings are superimposed.

The curves of the specific volumes of the *E*-broparestrol polymorphs as a function of temperature are almost parallel (see Fig. 5) and can be described by quadratic functions:

$$v_{I\text{-}E}/cm^3g^{-1} = 0.7149 + 5.610 \times 10^{-5} \times T/K + 1.739 \times 10^{-7} \times (T/K)^2 (r^2 = 0.999) \quad (2)$$

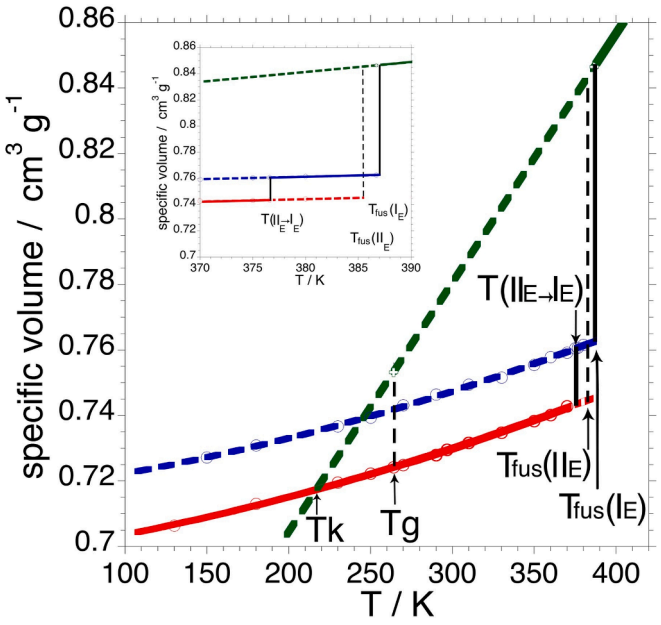

Fig. 5. Partial projection of the Helmholtz function on the *v*-*T* plane presenting the temperature dependence of the specific volumes of the condensed phases of *E*-broparestrol in equilibrium with their vapour. Blue: form I_E, red: form II_E, dark green: liquid, vertical bars: volume changes, dashed curves: metastable, solid curves: stable. T_k: Kauzmann temperature (216 K). Inset: detail of the volume changes between 370 K and 390 K.

$$v_{II-E}/cm^3g^{-1} = 0.6953 + 6.626 \times 10^{-5} \times T/K + 1.643 \times 10^{-7} \times (T/K)^2 (r^2 = 0.999) \quad (3)$$

They can also be fitted by straight lines:

$$v_{I-E}/cm^3g^{-1} = 0.7029 + 0.0001512 \times T/K (r^2 = 0.993)$$

$$v_{II-E}/cm^3g^{-1} = 0.6846 + 0.0001537 \times T/K (r^2 = 0.993)$$

Using equations (2)' and 3', the expansivities of forms I_E and II_E are: $\alpha_{V,I\text{-}E} = 2.15 \times 10^{-4}$ K^{-1} and $\alpha_{V,II\text{-}E} = 2.25 \times 10^{-4}$ K^{-1}, close to the value of about 2×10^{-4} K^{-1} usually found for molecular solids. (Céolin and Rietveld, 2015; Rietveld and Céolin, 2015; Gavezzotti, 2013).

3.1.4. Topological pressure–temperature phase diagram accounting for the dimorphism of E-broparestrol

According to the Le Chatelier principle, the $II_E \rightarrow I_E$ transition, which occurs endothermically on heating, should be favored by a temperature increase. In addition, since the specific volume of form II_E is smaller than that of form I_E, the $I_E \rightarrow II_E$ transition should be favored by an increase of pressure. In other words, the slope dP/dT of the I_E-II_E equilibrium should be positive with form I_E stable at high temperature and low pressure, while form II_E is the low-temperature, high-pressure phase. Two cases among the four pressure–temperature phase diagrams formerly drawn by Bakhuis-Roozeboom (Bakhuis Roozeboom, 1901) can accommodate such phase behaviour leading to two possible topological phase diagrams: either the I_E-liquid curve is steeper than the II_E-I_E curve (Roozeboom's case I, in which monotropic behavior replaces enantiotropic behavior on increasing pressure), or the II_E-I_E curve is steeper than the I_E-liquid curve (Roozeboom's case 2, which corresponds to an overall enantiotropic behavior). In the latter case, both polymorphs exhibit their own stable phase region irrespective of the pressure.

To determine which case is applicable for the dimorphism of *E*-broparestrol, a topological *P*-*T* phase diagram is constructed using the Clapeyron equation:

$$\frac{dP}{dT} = \frac{\Delta H}{T\Delta v} \quad (4)$$

and the following assumptions:

(1) The expansivity, α_V, of a molecular liquid is in the order of 1.2×10^{-3} K^{-1}. (Céolin and Rietveld, 2015; Rietveld and Céolin, 2015; Gavezzotti, 2013).

(2) Molecular liquids expand or shrink linearly: $v(T) = v_0 (1 + \alpha_V \times T)$, with T in K, near the melting temperature, T_{fus}, and below while cooling the metastable liquid.

(3) The ratio v_{liquid}/v_{cryst} is 1.11 at the melting temperature, approximating the solid–liquid-vapour triple point temperature. (Céolin and Rietveld, 2015; Rietveld and Céolin, 2015; Barrio et al., 2019; Goodman et al., 2004).

(4) The ratio v_{glass}/v_{cryst} is 1.06 at the glass transition temperature T_g. (Barrio et al., 2019).

Using **Eq. (2)**, the specific volume of form I_E at $T_{fus,I\text{-}E} = 386.7$ K is $v_{I\text{-}E} = 0.7626$ cm^3 g^{-1}. With assumption (3), the specific volume of the liquid at the melting point is found to be $v_{liq} = 0.8465$ cm^3 g^{-1} leading to a volume change of $v_{liq} - v_{I\text{-}E} = 0.0839$ cm^3 g^{-1} at $T_{fus,I\text{-}E}$.

Using **Eq. (3)**, the specific volume of form II_E is found to be 0.7242 cm^3 g^{-1} at $T_g = 264$ K, the glass transition temperature, where form II_E is stable. With assumption (4), the specific volume of the metastable liquid at T_g is found to be 0.7677 cm^3 g^{-1}.

With these two values of the spectific volume of the liquid and assumption (2), linear expansion, the dependence of the specific volume of the liquid on the temperature is found to be:

$$v_{liq}/cm^3g^{-1} = 0.598 + 0.000642 \times T/K \quad (5)$$

which leads, for the liquid, to an expansivity $\alpha_{v,liq}$ of 1.07×10^{-3} K^{-1}, which is reasonably close to the generally admitted value of about 1.2×10^{-3} K^{-1} (assumption (1)).

Because the specific volumes are determined for conditions under which the condensed phases are in equilibrium with the vapour phase, it can be inferred that Fig. 5 is a partial projection of the Helmholtz function of the free energies of the condensed phases of *E*-broparestrol in equilibrium with the vapour on the *T*-*v* plane. With the volume changes at the phase equilibrium temperatures from this projection and the Clapeyron equation (Eq. (4), the Helmholtz projection can be changed into a *P*-*T* projection of the Gibbs function.

The initial value of the dP/dT slope of the I_E-liquid equilibrium curve is found to be 2.45 MPa/K. Similarly, the initial value of the slope for the melting equilibrium of II_E is 2.35 MPa/K. Using Eqs. (2) and (3) to determine the volume change associated with the $II_E \rightarrow I_E$ transition at 376.6 K, one obtains: $v_{I\text{-}E} - v_{II\text{-}E} = 0.7607 - 0.7435 = 0.0172$ cm^3 g^{-1}. Incorporating this value into the Clapeyron equation (**Eq. (4)** together with the transition enthalpy $\Delta H = 11.4$ J/g and the transition temperature, leads to $dP/dT = 1.76$ MPa/K for the slope of the II-I equilibrium curve.

Because the vapour pressures at triple points I_E-liquid–vapour, II_E-liquid–vapour and I_E-II_E-vapour are very small, their values can be taken equal to 0 MPa. It follows that the equations for the I_E-liquid, II_E-liquid and I_E-II_E equilibria, which are usually straight over for several hundreds of MPa, are:

$$I_E - liquid : P/MPa = 2.45 \times T/K - 947 \quad (6)$$

$$II_E - liquid : P/MPa = 2.35 \times T/K - 904 \quad (7)$$

$$I_E - II_E : P/MPa = 1.78 \times T/K - 664 \quad (8)$$

Setting **Eqs. (6) and (7)** equal, leads to the coordinates of the I_E-II_E-liquid triple point, since it is the point at which the I_E-liquid and II_E-liquid equilibrium curves cross. The values are T(I_E-II_E-liquid) = 417 K and P(I_E-II_E-liquid) = 73 MPa.

Since a third equilibrium curve, II_E-I_E, passes through triple point I_E-II_E-liquid, the $P = f(T)$ equation for this curve can be determined using the coordinates of triple points I_E-II_E-liquid above and I_E-II_E-vapour (T = 376.6 K, P ≈ 0). One obtains $P_{I\text{-}II}$/MPa = 1.83 × T/K −688/MPa, i.e. an equation close to **Eq. (8)**. Although these calculations have been carried out using approximations, it is clear that ΔH and Δv are both positive in going from form II_E to form I_E leading to a positive slope for the II_E-I_E phase equilibrium in the pressure–temperature phase diagram. Moreover, the enthalpy difference being relatively small and the specific volume difference relatively large, the slope of the II_E-I_E equilibrium is expected to be shallow, as the calculations demonstrate. The observation that the I_E-II_E-liquid triple point occurs at positive pressure is demonstrated by the shallower slope of the II_E-I_E equilibrium versus both the I_E-L and the II_E-L equilibria and by the observation that the two equilibria I_E-liquid and II_E-liquid intersect at positive pressure as calculated above.

From these results, it can be inferred that the *P*-*T* phase diagram for the dimorphism of *E*-broparestrol corresponds to the first case of Bakhuis-Roozeboom, which can be found in **Figure S5** in the **Supplementary Materials**. (Bakhuis Roozeboom, 1901) On increasing pressure, enantiotopic behaviour turns into monotropic behavior, with form II_E the sole stable solid phase at high pressure.

3.2. Thermodynamic studies of the binary phase diagram between the E- and Z-isomers of broparestrol

3.2.1. Preliminary studies of the triclinic form I_Z of Z-broparestrol

A specimen of triclinic *Z*-broparestrol form I_Z was heated at a rate of 5 K min^{-1} up to the molten state. The DSC curve (Fig. 6**, curve A**) contains only an endothermic effect 'a' with an onset at $T_{fus,I\text{-}Z} = 385.5$ (1.0) K and a melting enthalpy of $\Delta_{fus}H_{I\text{-}Z}$ of 91.4(1.8) J/g. By quenching the melt at 223 K, and immediately reheating at the rate of 5 K min^{-1}, a new DSC curve was recorded (Fig. 6**, curve B**), which contains a glass transition at T_g = 267 K (midpoint), followed by an exothermic

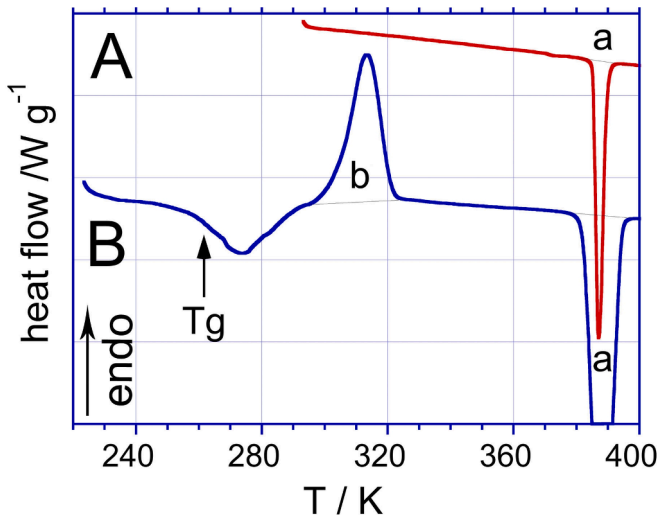

Fig. 6. DSC curves of *Z*-broparestrol recorded on heating at a rate of 5 K min^{-1} with (**A**) a sample of triclinic *Z*-broparestrol of which only the fusion was observed (endothermic peak 'a') and (**B**) immediately reheating the glass phase obtained after quenching a molten sample at 223 K. A glass transition, T_g, is recorded followed by an exothermic recristallisation 'b' and fusion 'a' at the same onset temperature as in (**A**).

recrystallization, event 'b' with an onset at 303.5 K ($\Delta_{cryst}H = -61.3$ J/g), and the melting peak 'a' at the same temperature and with the same melting enthalpy as obtained in the first run (**curve A**).

To confirm that the initial phase and the recrystallized one are the same, a powder of *Z*-broparestrol form I_Z was molten in a capillary tube then quickly cooled into the glass state. The X-ray diffraction pattern recorded immediately after recrystallization unambiguously demonstrated that the so-obtained solid was the same I_Z form as the initial one. Therefore, by contrast with the *E*-isomer, thermal treatment does not reveal any polymorphism for *Z*-broparestrol. It can be concluded however that the glass transition at 267 K for the *Z*-isomer agrees rather well with the empirical Tammann rule since it is found at $T_g/T_{fus} = 0.69$.

The temperature dependence of the lattice parameters of *Z*-broparestrol form I_Z has been determined between 130 K and 375 K (see **Table S9** in the **Supplementary Materials**), leading to the following specific volume as a function of the temperature:

$$v_{I-Z} = 0.6989 + 4.112 \times 10^{-5} \times T/K + 2.578 \times 10^{-7} \times (T/K)^2 (r^2 = 0.998) \quad (9)$$

From 130 K to 350 K, the temperature dependence of the specific volume can also be described by a linear function:

$$v_{I-Z} = 0.6858 + 0.0001624 \times T/K (r^2 = 0.994) \quad (10)$$

from which the expansivity $\alpha_{v,I\text{-}Z}$ of 2.4 × 10^{-4} K^{-1} is obtained. It is near the usual value of 2 × 10^{-4} K^{-1}. (Céolin and Rietveld, 2015; Rietveld and Céolin, 2015; Gavezzotti, 2013)

3.2.2. *The T-x phase diagram between forms II_E and I_Z of broparestrol*

DSC curves from the first series of experiments obtained with physical mixtures of forms II_E and I_Z annealed for one weak at 323 K are shown in **Figure S6a** in the **Supplementary Materials** together with the Tammann plot (**Figure S6b**) of the eutectic equilibrium ε_1 at 363(0.5) K. The related data have been compiled in **Table S10**, while the temperature-composition (*T-x*) phase diagram is presented in Fig. 7.

To determine the mole fraction $x_{\varepsilon 1}$ of the eutectic liquid, the intersection of the Tammann plot was determined using **Eqs. S1a** and **b** in the **Supplementary Materials**. By setting these equations equal, the mole fraction $x_{\varepsilon 1}$ of the eutectic liquid is found to be 0.423 (at $T_{\varepsilon 1} = 363$ K). Using the Schröder equation:

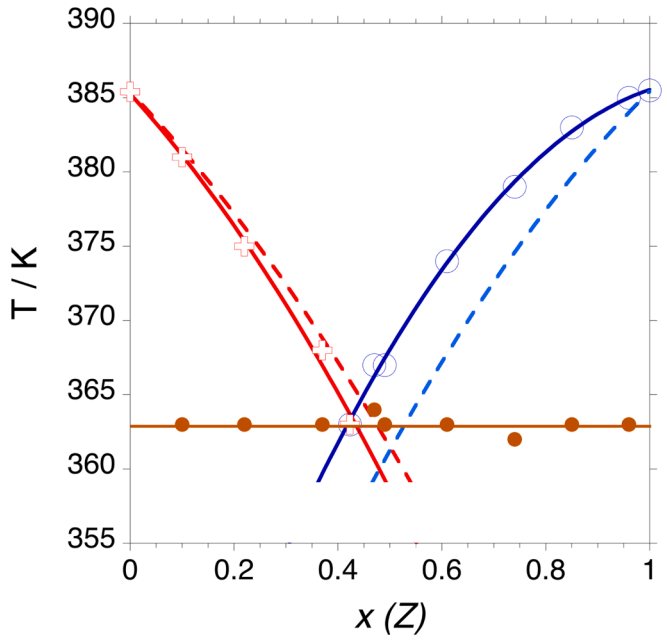

Fig. 7. *T-x* phase diagram involving form II_E and form I_Z of broparestrol after annealing one week at 323 K. Open crosses and open circles: experimental liquidus temperatures (**Table S10** in the **Supplementary Materials**), solid circles: experimental eutectic temperatures, solid curves: experimental liquidus curves rich in *E* (red) or *Z* (blue), dashed curves: ideal liquidus curves calculated by the Schröder equation (**Eq. (11)**) and straight horizontal line: eutectic equilibrium ε_1.

$$\ln x = \frac{\Delta_{fus}H}{R}\left(\frac{1}{T_{fus}} - \frac{1}{T_x}\right) \quad (11)$$

and the melting temperatures and melting enthalpies of the pure isomers, the two ideal liquidus curves (dashed lines in Fig. 7) have been determined. They cross at the ideal eutectic liquid coordinates: $x_{ideal} = 0.50$ and $T_{ideal} = 361$ K. The *Z*-rich liquidus curve does not behave ideally, whereas the *E*-rich liquidus remains near ideality.

3.2.3. *The T-x phase diagram between forms I_E and I_Z of broparestrol*

DSC curves obtained from this second series of experiments, obtained with samples homogenized by melting and recrystallisation on annealing for three years at room temperature, are available in the **Supplementary Materials Figure S7a** together with the Tammann plot (**Figure S7b** in the **Supplementary Materials**) of the eutectic equilibrium ε_2 at 358.1(1.1) K. The related data have been compiled in **Table S11** and the *T-x* phase diagram is shown in Fig. 8.

To determine the mole fraction $x_{\varepsilon 2}$ of the eutectic liquid, the intersection of the Tammann plot was determined with **Eqs. S2a** and **b** in the **Supplementary Materials**. By setting the two equations equal, the mole fraction $x_{\varepsilon 2}$ of the eutectic liquid is found to be 0.444. Using the Schröder equation (**Eq. (11)**) and the melting temperatures and melting enthalpies of the pure isomers, the two ideal liquidus curves (dashed curves in Fig. 8) have been determined. They cross at the ideal eutectic liquid coordinates: $x_{\varepsilon 2\text{-ideal}} = 0.49$ and $T_{\varepsilon 2\text{-ideal}} = 360$ K. It can be seen that the *E*-rich liquidus curve does not behave ideally. It may be tentatively ascribed to a narrow solid-solution range for form I_E as demonstrated by the DSC curve with sample $x_{I\text{-}Z} = 0.03$ (see **Figure S8a** in the **Supplementary Materials**) for which no eutectic peak is recorded.

3.2.4. *The T-x phase diagram between forms I_E and II_Z of broparestrol*

DSC curves obtained from the third series of experiments, obtained with samples homogenized by melting and recrystallisation during a few days at room temperature, are available in the **Supplementary**

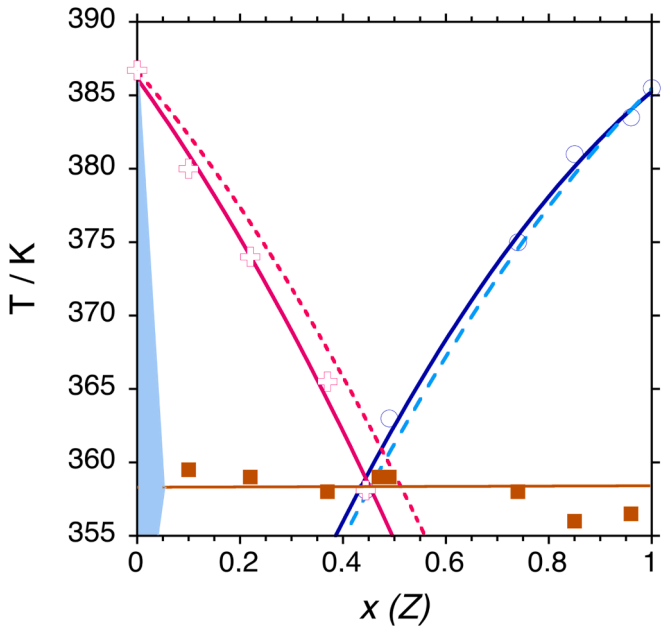

Fig. 8. *T-x* phase diagram involving forms I_E and I_Z after recrystallization for three years at room temperature. Open crosses and open circles: experimental liquidus temperatures (Table S11 in the **Supplementary Materials**), solid squares: experimental eutectic temperatures, solid curves: experimental liquidus curves rich in *E* (red) or *Z* (blue), dashed curves: ideal liquidus curves calculated by the Schröder equation (**Eq.** (11) and straight horizontal line: eutectic equilibrium ε_2. The tentative solid solution range involving high-temperature form I_E is shown in light blue, which may explain the non-ideality of the liquidus curve.

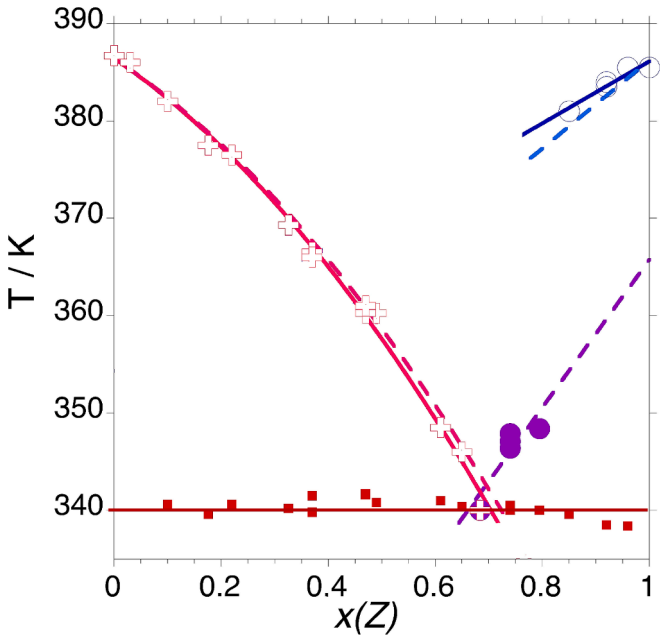

Fig. 9. Third *T-x* phase diagram involving form I_E and the metastable form II_Z of *Z*-broparestrol that recrystallizes into I_Z on the *Z*-rich side of the diagram. Open crosses and open circles: stable experimental liquidus temperatures (Table S12 in the **Supplementary Materials**), solid violet circles: metastable experimental liquidus temperatures of *Z*-probarestrol, solid squares: experimental eutectic temperatures, solid curves: experimental liquidus curves rich in *E* (red) or *Z* (blue), dashed curves: ideal liquidus curves calculated by the Schröder equation (**Eq.** (11) and straight horizontal line: eutectic equilibrium ε_3, violet dashed line: tentative representation of the liquidus curve involving the metastable polymorph of *Z*-broparestrol.

Materials: Figure S8**a** and close-ups of recrystallisation events in Figure S8**b**. The Tammann plot can be found in Figure S8**c** of the Supplementary Materials. It involves the eutectic equilibrium ε_3 at 340.2 K (onset). The related data have been compiled in Table S12 in the Supplementary Materials and the *T-x* phase diagram is shown in Fig. 9.

To determine the mole fraction $x_{\varepsilon 3}$ of the eutectic liquid, the intersection of the Tammann plot was determined with Eqs. S3**a** and **b** in the Supplementary Materials. By setting the two equations equal, the mole fraction $x_{\varepsilon 3}$ of the eutectic liquid is found to be 0.684. The corresponding melting enthalpy, $\Delta H_{\varepsilon 3}$, of 58.52 J/g is found at the intersection of the two lines in the Tammann plot (see Figure S8**c** in the Supplementary Materials).

The third *T-x* phase diagram in Fig. 9 demonstrates that the *E*-rich liquidus curve related to form I_E behaves almost ideally since the experimental curve and the ideal one, calculated with the Schröder equation (**Eq.** (11), are in close proximity. Moreover, the ideal liquidus curves for the *E*-rich parts in the first (Fig. 7) and in the third (Fig. 9) *T-x* phase diagrams cross at 377.7 K (see Figure S9 in the Supplementary Materials), which is virtually the same temperature as 376.6 K, calculated for the transition from form II_E to the high-temperature form I_E in section 3.1.1.

3.2.5. *Evidence for the dimorphism of Z-broparestrol*

The *Z*-rich liquidus in Fig. 9 behaves differently than the *E*-rich side: from the composition of the eutectic liquid $x_{\varepsilon 3} = 0.684$, a liquidus curve is observed (violet circles in Fig. 9) up to $x_Z = 0.795$. Then, it can be seen in Figures S8**a and b** of the Supplementary Materials that exothermic recrystallization occurs leading to the stable liquidus curve related to form I_Z.

Therefore, it can be concluded from the third *T-x* phase diagram that the *Z*-broparestrol isomer is at least dimorphic and that the new form (II_Z) melts at a lower temperature than the triclinic form. This is shown by the **tentatively** drawn liquidus curve (violet dashed line in Fig. 9 (see also values in bold italics in Table S12 in the Supplementary Materials) which extrapolates to $T \approx 366$ K at $x_Z = 1$ using a linear fit. It demonstrates that the new form, which could not be isolated for further characterization, is highly metastable.

Moreover, the total enthalpies reported in bold in Table S12 (in the Supplementary Materials) correspond to the change between an initial state consisting of solid forms $I_E + II_Z$ in fixed ratios and a final state consisting of an isotropic liquid with the same chemical composition. Therefore, Hess' law applies and the line that describes the total enthaly as a function of x_Z (see the equation in the caption of Figure S8**c** in the Supplementary Materials) can be extrapolated to $x_Z = 1$ leading to a value of 68.1 J/g, which can be **tentatively** considered as the enthalpy of fusion of the new metastable form II_Z of *Z*-broparestrol.

Concerning the transition from the stable triclinic form I_Z to the metastable form II_Z, it is inferred from Hess' law that it endothermically shifts right on heating with $\Delta_{IZ \rightarrow IIZ}H = +23.3$ J/g. In addition, using the formula proposed by Yu (**Eq.** (1), (Yu, 1995) it is found that the equilibrium is located at about 466–471 K K. In other words, this indicates that the I_Z-II_Z-vapour triple point is in a region of the *P-T* phase diagram of *Z*-broparestrol where the liquid phase is stable. Unfortunately, it cannot be determined whether form II_Z becomes stable on increasing the pressure, or whether it is a case of overall metastability, since nothing is known about the specific volume of form II_Z. In contrast to the case the *E*-isomer dimorphism, it can be concluded that form II_Z behaves monotropically at ordinary pressure.

4. Concluding remarks

The physicochemical study of the two isomers of broparestrol has revealed dimorphism for both isomers in contrast to the results reported by Dvolaitzky and Jacques who did not demonstrate any polymorphism

of the components while studying similar binary systems by DSC. (Dvolaitzky and Jacques, 1958).

The crystal structure of the *E*-isomer form I_E was solved at room temperature with the help of high-resolution X-ray powder diffraction. It was demonstrated that it corresponds to a high-temperature form that persists at room temperature for several days. In addition, the phase relationship between the two forms was inferred from the topological pressure–temperature phase diagram, which was found to be similar to the case of sulfur, i.e. enantiotropic behavior that turns monotropic on increasing pressure.

By contrast, the existence of the dimorphism of the *Z*-isomer was unexpectedly revealed by a DSC study of *Z*-rich mixtures in the *T*-*x* binary phase diagram between the two isomers. Although the polymorph could not be isolated for crystal structure determination, it was inferred that it melts at a lower temperature than the known form I_Z and that it possesses a monotropic relationship with this form at ordinary pressure. An overview of the available thermodynamic and crystallographic information of the two series of broparestrol polymorphs have been compiled in Table 1.

Three experimental *T*-*x* phase diagrams have been established each with an invariant eutectic equilibrium at 363 K, 358 K, and 340 K. None of these three diagrams fully represents stable behaviour as explained below.

The *T*-*x* phase diagram in section 3.2.2 exhibits a eutectic equilibrium between the low-temperature form II_E and form I_Z. Since the fusion of form II_E is metastable and it does not transform endothermically into form I_E on heating, the diagram cannot be fully stable. Moreover, it is not clear whether the *Z*-rich liquidus curve is in equilibrium since preliminary annealing took only a short time, which may not have been enough to properly homogenize the *Z*-rich mixtures.

The *T*-*x* phase diagram in section 3.2.3 exhibits a eutectic mixture of the high-temperature form I_E and form I_Z. This indicates that recrystallization after melting leads to the high-temperature form I_E, which did not transform back to the stable room-temperature form II_E on cooling. Therefore, this second *T*-*x* phase diagram is not fully stable either. Moreover, the *Z*-rich liquidus is found to be different from that of the first *T*-*x* diagram and close to ideality.

The *T*-*x* phase diagram in section 3.2.4 exhibits a eutectic equilibrium between the high-temperature form I_E and the metastable form II_Z with recrystallization into the stable form I_Z in the *Z*-rich liquidus region. Again, this third *T*-*x* phase diagram cannot represent a stable diagram.

To sum up, (1) three partly metastable phase diagrams have been obtained from the four possible combinations involving one of the following isomeric polymorph pairs: I_E-I_Z, I_E-II_Z, II_E-I_Z, and II_E-II_Z. (2) The stable phase diagram exhibits the II_E-I_E transition at about 366 K, as shown in Fig. 10 (see also **Eqs. S4 and S5** and **Figure S10** in the **Supplementary Materials**), and the *E*-sided liquidus curve consists of two parts: at lower temperatures, a liquid in equilibrium with form II_E and at higher temperatures a liquid in equilibrium with form I_E. With the empirical equations of the experimental liquidus curves $L_{II\text{-}E}$ and $L_{I\text{-}E}$, one finds that they cross at $x_Z = 0.391$ and $T = 365.7$ K (**Eqs. S4 and S5**).

Since the observed temperature is lower by about 10 degrees than the calculated one for the phase transition involving the pure polymorphs (376.6 K, cf **Figure S9** in the **Supplementary Materials**), two conclusions can be drawn:

(1) The invariant equilibrium involving forms I_E, II_E, and the liquid Lμ ($x_Z = 0.391$) is a metatectic equilibrium (see **Figure S10** in the **Supplementary Materials**), written as: (Hillert, 2008).

II_E + Liquid Lμ ⇔ I_E, on heating.

(2) The inequality in the extent of the limited thermodynamic solid solutions at the invariant temperature shows that the amount of *Z* molecules as an impurity in form I_E should be larger than for form II_E (**Figure S10** in the **Supplementary Materials**). It entails that the specific volume of form I_E is greater than that of form II_E. This coincides with the inequality in the specific volumes $V_{cell}(I_E) = 1800$ Å^3 > $V_{cell}(II_E) = 1764$ Å^3 at 293 K and strengthens the assumption that the less dense phase can incorporate a larger amount of impurities.

The absence of a eutectic peak in the DSC curve of the sample $x_Z = 0.03$ (see **Figure S8a** in the **Supplementary Materials**) is an experimental indication in favor of the existence of a limited solid solution for form I_E, while this is not the case in the DSC curve of specimen $x_Z = 0.96$ which clearly exhibits a weak endotherm accounting for a eutectic equilibrium (**Figures S8a and b** in the **Supplementary Materials**). By contrast, on the *Z*-rich side, only a liquidus curve in equilibrium with form I_Z (as in Fig. 8) is found due to the monotropic behavior of form II_Z.

By setting the equations of the experimental low-temperature *E*-sided and *Z*-sided liquidus curves equal, one finds the coordinates $x_{Z\varepsilon} =$

Table 1
Thermodynamic and crystallographic information on the four solid phases found in Broparestrol.

Property	*E*-broparestrol		*Z*-broparestrol	
	Form I_E	Form II_E	Form I_Z	Form II_Z
Formula, Molar mass *M*/ g/mol	$C_{22}H_{19}Br$, 363.31			
T_{fus} /K	386.7	385.4	385.5	363-366[a]
$\Delta_{fus}H$ /J/g	79.4	90.8	91.4	68.1[a]
T_g /K	264		267	
$\Delta_{II\rightarrow I}H$ /J/g	11.4[b]		23.3[a]	
$T_{II\rightarrow I}$ /K	376.6[b]		466-471[a]	
System, space group	Monoclinic $P2_1/c$	Monoclinic $P2_1/c$,	Triclinic *P*-1	unknown
V_{cell} /A^3, Z, T /K	1799.6, 4, 293	1784.0, 4, 293	883.2, 2, 293	unknown
Density /g cm^{-3} (293 K)	1.341	1.372	1.366	unknown
Expansivity α_V/ K^{-1}	2.15×10^{-4}	2.25×10^{-4}	2.4×10^{-4}	unknown

[a] by 'tentative' extrapolation
[b] calculated.

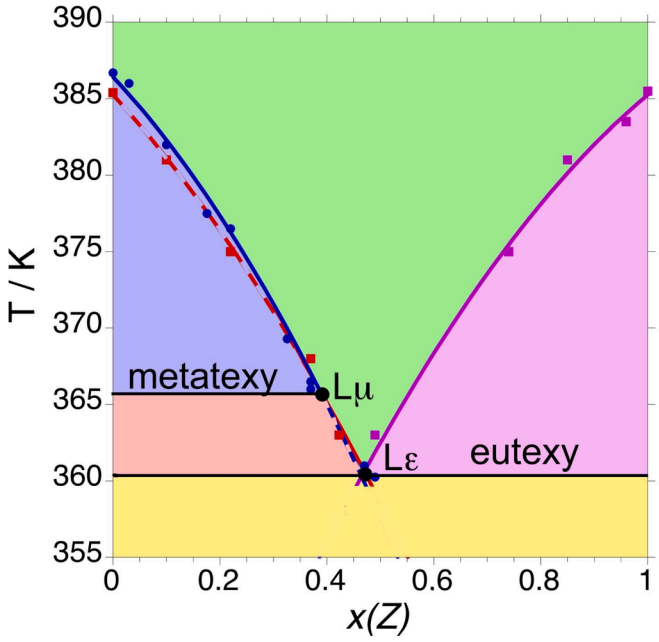

Fig. 10. Stable *T*-*x* phase diagram between *E*- and *Z*-isomers of broparestrol. Blue area: form I_E and liquid, red area: form II_E and liquid, violet area: form I_Z + liquid, green area: liquid, yellow area: form II_E and form I_Z, dashed curves are metastable, metatexy = invariant equilibrium [form II_E + Liquid Lμ ⇔ form I_E], on heating and eutexy = invariant equilibrium [form II_E + form I_Z ⇔ liquid Lε] on heating. For the sake of clarity, the limited solid solutions on the *E*-rich side have not been represented in the graph. A graph in which the domain with solid solutions has been enlarged is available in **Figure S10** in the **Supplementary Materials**.

0.470 and $T_\varepsilon = 360.6$ K for the eutectic liquid Lε of the invariant eutectic equilibrium on heating:

form II_E + form $I_Z \Leftrightarrow$ liquid Lε.

CRediT authorship contribution statement

Siro Toscani: Writing – review & editing, Validation, Investigation, Formal analysis. **Hassan Allouchi:** Validation, Investigation, Formal analysis. **René Ceolin:** Writing – review & editing, Writing – original draft, Investigation, Formal analysis, Conceptualization. **Laia Villalobos:** Investigation. **Maria Barrio:** Supervision, Methodology, Investigation, Formal analysis. **Josep-Lluis Tamarit:** Writing – review & editing, Supervision, Resources, Funding acquisition. **Ivo B. Rietveld:** Writing – review & editing, Writing – original draft, Validation, Investigation, Conceptualization.

Declaration of competing interest

The authors declare the following financial interests/personal relationships which may be considered as potential competing interests: J.-Ll. Tamarit reports financial support was provided by Spanish ministry of science and innovation. J.-Ll. Tamarit reports financial support was provided by Government of Catalonia. If there are other authors, they declare that they have no known competing financial interests or personal relationships that could have appeared to influence the work reported in this paper.

Acknowledgements

This work was partially supported by the Spanish Ministry of Science and Innovation under projects PID2023-146623NB-I00 and CEX2023-001300 and by the Generalitat de Catalunya (2021SGR00343).

Appendix A. Supplementary material

Supplementary data to this article can be found online at https://doi.org/10.1016/j.ijpharm.2024.125060.

Data availability

Data will be made available on request.

References

Al-Hassan, M.I., 1987. A one-step synthesis of broparestrol. Synthesis 1987 (09), 815–816.
Al-Hassan, M.I., 1987. Synthesis of broparestrol using palladium-catalyzed cross-coupling. J. Organomet. Chem. 321 (1), 119–121.
Bakhuis Roozeboom, H. W., 1901. *Die heterogenen Gleichgewichte vom Standpunkte der Phasenlehre. Erstes Heft: Die Phasenlehre - Systeme aus einer Komponente.* Friedrich Vieweg und Sohn: Braunschweig; Vol. 1.
Barrio, M., de Oliveira, P., Céolin, R., Lopez, D.O., Tamarit, J.L., 2002. Polymorphism of 2-methyl-2-chloropropane and 2,2-dimethylpropane (neopentane): thermodynamic evidence for a high-pressure orientationally disordered rhombohedral phase through topological p-T diagrams. Chem. Mater. 14 (2), 851–857.
Barrio, M., Allouchi, H., Tamarit, J.L., Ceolin, R., Berthon-Cedille, L., Rietveld, I.B., 2019. Experimental and topological determination of the pressure-temperature phase diagram of racemic etifoxine, a pharmaceutical ingredient with anxiolytic properties. Int. J. Pharm. 572, 118812.
Bolla, G., Nangia, A., 2016. Pharmaceutical cocrystals: walking the talk. Chem. Commun. 52 (54), 8342–8360.
Boultif, A., Louër, D., 1991. Indexing of powder diffraction patterns for low-symmetry lattices by the successive dichotomy method. J. Appl. Crystallogr. 24, 987–993.
Brandel, C., Amharar, Y., Rollinger, J.M., Griesser, U.J., Cartigny, Y., Petit, S., Coquerel, G., 2013. Impact of molecular flexibility on double polymorphism, solid solutions and chiral discrimination during crystallization of diprophylline enantiomers. Mol. Pharmaceut. 10 (10), 3850–3861.
Bruno, I.J., Cole, J.C., Kessler, M., Jie, L., Motherwell, W.D.S., Purkis, L.H., Smith, B.R., Taylor, R., Cooper, R.I., Harris, S.E., Orpen, A.G., 2004. Retrieval of crystallographically-derived molecular geometry information. J. Chem. Inf. Comput. Sci. 44, 2133–2144.
Buu Hoï, N.P., 1946. La chimie des hydrocarbures oestrogènes. *Bulletin de la Société Chimie de France*, 117-123.
Céolin, R., Rietveld, I.B., 2015. The topological pressure-temperature phase diagram of ritonavir, an extraordinary case of crystalline dimorphism. Ann. Pharm. Fr. 73 (1), 22–30.
Coelho, A.A., 2003. Indexing of powder diffracton patterns by iterative use of singular value decomposition. J. Appl. Crystallogr. 36, 86–95.
Coelho, A., 2018. TOPAS and TOPAS-academic: an optimization program integrating computer algebra and crystallographic objects written in C++. J. Appl. Crystallogr. 51 (1), 210–218.
Coelho, A.A., 2007. *TOPAS Academic version 4.1 (Computer Software)*, Coelho Software: Brisbane.
Coquerel, G., 2006. Preferential crystallization. In *Novel Optical Resolution Technologies*, Sakai, K.; Hirayama, N.; Tamura, R., Eds. Springer, Berlin: Heidelberg, Vol. 269, pp 1-51.
David, W.I.F., Sivia, D.S., 2001. Background estimation using a robust Bayesian analysis. J. Appl. Crystallogr. 34, 318–324.
David, W.I.F., Shankland, K., van de Streek, J., Pidcock, E., Motherwell, W.D.S., Cole, J. C., 2006. DASH: a program for crystal structure determination from powder diffraction data. J. Appl. Crystallogr. 39, 910–915.
Drosdowsky, M., Edery, M., Guggiari, M., Montes-Rendon, A., Rudali, G., Vives, C., 1980. Inhibition of prolactin-induced mammary cancer in C3Hf (XVII) mice with the trans isomer of bromotriphenylethylene1. Cancer Res 40 (5), 1674–1679.
Dvolaitzky, M., Jacques, J., 1958. Structure moléculaire et activité oestrogène (XV): etude de quelques dérivés du triphényl-1,2,2-bromo-2-éthylène. Bull. Soc. Chim. Biol. 40 (5–6), 939–953.
Finger, L.W., Cox, D.E., Jephcoat, A.P., 1994. A correction for powder diffraction peak asymmetry due to axial divergence. J. Appl. Crystallogr. 27, 892–900.
Fornies-Marquina, J.M., Courseille, C., Busetta, B., Hospital, M., 1972. 1-Bromo-2-(p-ethylphenyl)-1,2-diphenylethylene. Cryst. Struct. Commun. 1 (3), 261–264.
Gavezzotti, A., 2013. *Molecular Aggregation. Structure Analysis and Molecular Simulation of Crystals and Liquids*. Oxford University Press: Oxford, UK.
Goodman, B.T., Wilding, W.V., Oscarson, J.L., Rowley, R.L., 2004. A note on the relationship between organic solid density and liquid density at the triple point. J. Chem. Eng. Data 49 (6), 1512–1514.
Haget, Y., Chanh, N.B., Meresse, A., Bonpunt, L., Michaud, F., Negrier, P., Cuevas-Diarte, M.A., Oonk, H.A.J., 1999. Isomorphism and mixed crystals in 2-R-naphthalenes: evidence of structural subfamilies and prediction of metastable forms. J. Appl. Crystallogr. 32, 481–488.
Hillert, M., 2008. *Phase Equilibria, Phase Diagrams and Phase Transformations, Their Thermodynamic Basis*. 2nd ed.; Cambridge University Press: Cambridge UK, p 262.
Jacques, J., Collet, A., Wilen, S.H., 1994. *Enantiomers, Racemates, and Resolutions*. Krieger Publishing Company: Malabar FL.
Jain, S., Patel, N., Lin, S., 2015. Solubility and dissolution enhancement strategies: current understanding and recent trends. Drug Dev. Ind. Pharm. 41 (6), 875–887.
Johnston, J.N., Henter, I.D., Zarate, C.A., 2023. The antidepressant actions of ketamine and its enantiomers. Pharmacol. Therap. 246, 108431.
Kawakami, K., Harada, T., Miura, K., Yoshihashi, Y., Yonemochi, E., Terada, K., Moriyama, H., 2014. Relationship between crystallization tendencies during cooling from melt and isothermal storage: toward a general understanding of physical stability of pharmaceutical glasses. Mol. Pharmaceut. 11 (6), 1835–1843.
Kissi, E.O., Khorami, K., Rades, T., 2019. Determination of stable co-amorphous drug–drug ratios from the eutectic behavior of crystalline physical mixtures. Pharmaceutics 11 (12), 628.
Laroche, M.S.L., 1978. Nouvelle composition therapeutique à base de trans-broparestrol. FR2383665B1, 24/10/1980.
Markvardsen, A.J., David, W.I.F., Johnson, J.C., Shankland, K., 2001. A probabilistic approach to space-group determination from powder diffraction data. Acta Crystallogr. A 57, 47–54.
Mutiti, C.S., Kapungu, N.N., Kanji, C.R., Stadler, N., Stingl, J., Nhachi, C., Hakim, J., Masimirembwa, C., Thelingwani, R.S., 2021. Clinically relevant enantiomer specific R- and S-praziquantel pharmacokinetic drug-drug interactions with efavirenz and ritonavir. Pharmacol. Res. Perspect. 9 (3), e00769.
Nyamba, I., Lechanteur, A., Semdé, R., Evrard, B., 2021. Physical formulation approaches for improving aqueous solubility and bioavailability of ellagic acid: a review. Eur. J. Pharm. Biopharm. 159, 198–210.
Pardo, L.C., Barrio, M., Tamarit, J.L., López, D.O., Salud, J., Négrier, P., Mondieig, D., 2001. First experimental demonstration of crossed isodimorphism: (CH3)3CCl + CCl4 melting phase diagram. Phys. Chem. Chem. Phys. 3 (13), 2644–2649.
Pardo, L.C., Barrio, M., Tamarit, J.L., López, D.O., Salud, J., Oonk, H.A.J., 2005. Orientationally Disordered Mixed Crystals Sharing Methylchloromethanes [(CH3)4-nCCln, n = 0, …, 4]. Chem. Mater. 17, 6146–6153.
Qiao, N., Li, M., Schlindwein, W., Malek, N., Davies, A., Trappitt, G., 2011. Pharmaceutical cocrystals: an overview. Int. J. Pharm. 419 (1), 1–11.
Rietveld, I.B., Céolin, R., 2015. Phenomenology of crystalline polymorphism: overal monotropic behavior of the cardiotonic agent FK664 forms A and B. J. Therm. Anal. Calorim. 120 (2), 1079–1087.
Rietveld, I.B., Barrio, M., Do, B., Tamarit, J.L., Ceolin, R., 2012. Overall stability for the ibuprofen racemate: experimental and topological results leading to the pressure-temperature phase relationships between its racemate and conglomerate. J. Phys. Chem. B 116 (18), 5568–5574.
Rodier, N., Ceolin, R., Dubois, P., Fournival, J.L., 1989. (Z)-broparestrol. Acta Crystallogr. Sect. C Struct. Chem. 45 (9), 1455–1457.

Thompson, P., Cox, D.E., Hastings, J.B., 1987. Rietveld refinement of Debye-Scherrer synchrotron X-ray data from Al_2O_3. J. Appl. Crystallogr. 20, 79–83.
Valenti, S., Cazorla, C., Romanini, M., Tamarit, J.L., Macovez, R., 2023. Eutectic mixture formation and relaxation dynamics of coamorphous mixtures of two benzodiazepine drugs. Pharmaceutics 15 (1), 196.
Yu, L., 1995. Inferring thermodynamic stability relationship of polymorphs from melting data. J. Pharm. Sci. 84 (8), 966–974.